Available online at www.sciencedirect.com

ScienceDirect

journal homepage: http://www.elsevier.com/locate/acme

Original Research Article

Stress field determination based on digital image correlation results

Sandra Musial, Marcin Nowak, Michal Maj *

Institute of Fundamental Technological Research, Polish Academy of Sciences, Pawinskiego 5B, 02-106 Warsaw, Poland

ARTICLE INFO

Article history:
Received 18 January 2019
Accepted 9 June 2019
Available online 3 July 2019

Keywords:
Stress field determination
Digital image correlation (DIC)
Finite element analysis (FEA)
Elastoplastic constitutive model
Plastic work

ABSTRACT

The aim of this work was to determine the stress distribution during plastic deformation, based on the displacement field obtained using the digital image correlation (DIC) method. To achieve stress distribution, the experimentally measured displacement gradient and the elastoplastic material model with isotropic hardening were used. The proposed approach was implemented in the ThermoCorr program. The developed procedure was used to determine stress fields for uniaxial tension and simple shear processes, carried out on samples made of austenitic steel 304L. Both material parameters, such as the Young's modulus, Poisson's ratio, yield stress, and parameters of the hardening curve, were acquired experimentally. The macroscopic force obtained from the DIC-based stresses and its finite element analysis (FEA) equivalent were compared with that measured during the experiment. It was shown that the DIC-based approach gives more accurate results with respect to FEA, especially for a simple shear test, where FEA significantly overestimates the value of experimentally obtained macroscopic force.

1. Introduction

In recent years, the digital image correlation (DIC) has become one of the most used full-field optical methods of displacement measurement in the field of experimental solid mechanics [1]. The method has been extensively investigated by many researchers, and as a result the efficiency and accuracy of calculations has been significantly improved [2,3] and the application range has been greatly expanded, e.g. in shape measurement [4] and calibration of concrete parameters [5]. In addition to displacement measurement, the DIC method has been extended for estimating strain distributions, which are important and desirable in many experimental analyses [6]. The DIC has recently proven to be an efficient technique to experimentally evaluate a broad set of elastic constants of anisotropic materials [7,8]. The authors in Refs. [9,10] used the DIC to study the strain field within the Portevin–Le Chatelier (PLC) bands. Displacement and strain fields obtained using the DIC method have been utilized to analyze damage mechanisms in Ref. [11]. Having measured strains, new questions arise. Is it possible to determine the stress distribution on the basis of the DIC results? Unfortunately, stress state cannot be directly computed from the DIC data because some predefined constitutive law together with the known material parameters should be specified. In the case of the linear elasticity,

* *Corresponding author.*
E-mail addresses: smusial@ippt.pan.pl (S. Musial), nowakm@ippt.pan.pl (M. Nowak), mimaj@ippt.pan.pl (M. Maj).
https://doi.org/10.1016/j.acme.2019.06.007
1644-9665/

List of symbols

$\boldsymbol{\sigma}$	Cauchy stress tensor
$\boldsymbol{\varepsilon}$	Hencky strain tensor
$\boldsymbol{\varepsilon}^e$	elastic part of the Hencky strain tensor
$\boldsymbol{\varepsilon}^p$	plastic part of the Hencky strain tensor
w^e	elastic work
w^p	plastic work
E	Young's modulus
ν	Poisson's ratio
σ_y	yield stress
$\mathbf{x} = (x,y)$	Eulerian coordinates
$\mathbf{X} = (X,Y)$	Lagrangian coordinates
$\mathbf{H}$	displacement gradient tensor
$\mathbf{F}$	deformation gradient tensor
$\mathbf{U}$	stretch tensor
$\mathbf{C}$	deformation tensor
$I_1^U,\ I_2^U,\ I_3^U$	first, second and third invariant of the stretch tensor
$\mathbf{D}$	stiffness matrix
ε^p	equivalent plastic strain
σ_{HM}	Huber–von Mises stress

knowledge of the stiffness tensor makes it possible to determine the stresses by simply multiplying the stiffness tensor by the strain tensor. However, the majority of materials require more sophisticated material models that cannot be limited to the linear elasticity, e.g. materials that exhibit a plastic (irreversible) range. In a traditional mechanical test this problem can be solved when the stress and strain fields are uniform. In this case the stress can be determined from the loads applied to the specimen, taking into account the specimen geometry. However, often either the strain becomes non-uniform as a result of localization [12,13] or the specimen is designed or constrained to obtain non-uniform deformation [14]. Generally, there seems to be lack of literature concerning stress field determination directly from DIC results. One of the most widely used approaches combines finite element analysis (FEA), DIC and numerical optimization to determine constitutive parameters of the assumed material model. During the optimization process, the parameters of the model are updated until the measured displacement distribution using DIC is close enough to that from FEA simulation [15]. The DIC method is also used with the hole drilling method for determining residual stresses [16,17]. It was implemented as an alternative to the tensometric rosettes based version. A different method of stress field estimation was described in another study [18], which aimed to determine the energy storage rate distribution in the area of strain localization using infrared and visible imaging. The stress field was obtained from the force measured by the testing machine taking into account actual sample geometry assuming constant stress in the cross section. Similar analysis was applied in the work [19] in order to determine the stress–strain relation during tensile of an anisotropic titanium. In the paper [20] the authors presented methodology of characterizing the material behaviour at the point of fracture. The stress–strain curve was evaluated using DIC data and the stepwise modelling method. However, the approach was not used for the full-field stress analysis, what was the main goal of the paper [21], where simplified solution of the plastic flow rule equation was used for stress determination. Nevertheless, the statement made by the authors, that plastic strain can be easily derived from the DIC data, seems to be not true and there are no details how it was done in the paper.

This work presents a new approach of direct stress calculation using DIC data. The DIC-based stresses are calculated with a predefined elastic-plastic constitutive model in which parameters were estimated using a traditional mechanical tensile test. The developed numerical algorithm allows the decomposition of the total strain into its elastic and plastic parts. Numerical simulations and optimization are not required. The algorithm has been applied for the experimental data obtained during uniaxial tension and simple shear tests. Moreover, the obtained stress distributions were compared with the FEA assuming the same constitutive model. The considerations have been limited to the 2D DIC only. Nevertheless, the extension to the 3D DIC [22] or digital volume correlation (DVC) [23] is straightforward.

2. DIC-based stress determination

The analysis presented below concerns two-dimensional case, therefore 2D DIC, and the plane stress condition were applied. In the proposed approach the experimentally obtained evolution of the field of displacement gradient and J_2 plasticity constitutive model are used for determining stress distribution. The displacement gradient tensor $\mathbf{H}$ obtained from the 2D DIC analysis has the following form:

$$\mathbf{H} = \frac{\partial \mathbf{u}}{\partial \mathbf{X}} = \begin{bmatrix} \frac{\partial u_x}{\partial X} & \frac{\partial u_x}{\partial Y} & 0 \\ \frac{\partial u_y}{\partial X} & \frac{\partial u_y}{\partial Y} & 0 \\ 0 & 0 & [\cdot] \end{bmatrix} \tag{1}$$

where $\mathbf{u} = (u_x, u_y)$ is the displacement vector and $\mathbf{X} = (X,Y)$ is a position of a material point in the Lagrangian coordinate system. The $\partial u_z/\partial Z$ and corresponding ε_{zz} strain component, which is not measured in 2D DIC analysis, is usually calculated under assumption of a constant volume. Here, the ε_{zz} component is calculated iteratively to ensure the plane stress condition. A variety of strain measures can be calculated using the $\mathbf{H}$ tensor, obtained directly by the differentiation of displacement field.

In the first step, the Hencky strain (true strain) tensor was chosen and was calculated for each instant of the deformation process. The calculations include obtaining the deformation gradient $\mathbf{F} = \mathbf{H} + \mathbf{I}$ (where $\mathbf{I}$ is the 3×3 identity matrix), the deformation tensor $\mathbf{C} = \mathbf{F}^T\mathbf{F}$ and the stretch tensor $\mathbf{U} = \sqrt{\mathbf{C}}$. The stretch tensor was calculated using the Cayley–Hamilton theorem:

$$\mathbf{U} = \sqrt{\mathbf{C}} = \frac{\mathbf{C}^2 - \left((I_1^U)^2 + I_2^U\right)\mathbf{C} - I_1^U I_3^U \mathbf{I}}{I_1^U I_2^U + I_3^U}. \tag{2}$$

where I_1^U, I_2^U, I_3^U are the first, second and third stretch tensor invariants, respectively. Next, the Hencky strain tensor was obtained using following formula:

$$\boldsymbol{\varepsilon} = \ln \mathbf{U} = \sum_{n=1}^{\infty} \frac{(-1)^{n-1}}{n} (\mathbf{U}-\mathbf{I})^n. \tag{3}$$

The initial conditions for the process are defined as follows:

$$\boldsymbol{\sigma}_0 = 0, \quad \boldsymbol{\varepsilon}_0^e = 0, \quad \boldsymbol{\varepsilon}_0^p = 0, \quad \bar{\varepsilon}_0^p = 0, \tag{4}$$

where $\boldsymbol{\sigma}$ is the Cauchy stress tensor, $\boldsymbol{\varepsilon}^e$ and $\boldsymbol{\varepsilon}^p$ are the elastic and plastic part of the Hencky strain tensor, respectively, and $\bar{\varepsilon}^p$ is the equivalent plastic strain.

The evolution of the stress tensor is calculated using an elastic-plastic material model with isotropic hardening. At the beginning of each calculation step, the trial elastic stress is obtained using isotropic Hooke's law. Then, the plasticity condition is checked (whether the step is elastic or plastic) according to the Huber–von Mises yield criterion. If the deformation is elastic, the trial stress is correct and the procedure is closed; otherwise, the final stress is calculated using the return mapping algorithm [24]. For the plane stress condition, the modified ε_{zz} component is also returned. Finally, the calculated stress, elastic and plastic parts of the strain and equivalent plastic strain are saved and are treated as a new input for the next calculation step. A flowchart of the presented DIC-based stress calculation algorithm is shown in Fig. 1. The loop contained in the flowchart is executed for every point of DIC analysis. The described procedure was implemented in ThermoCorr software [25], designed for determining coupled displacement and temperature fields.

The procedure was validated throughout the comparison between the obtained stress distributions and stress distributions computed using the ABAQUS FE program. In the first step, a square area (see grey square in Fig. 2a) was discretized by finite elements. Then, according to the positions of integration points, the set of points in DIC-based analysis was defined. Next, the known, virtual non-uniform displacement field was applied onto the initial configuration numerically (see green area in Fig. 2a). In FEA, for each node of the mesh, the generated displacement was applied as a prescribed displacement boundary condition. In DIC-based approach, the displacement gradient was derived and the procedure shown in the flow chart in Fig. 1 was applied. The elastic-plastic material model with following parameters: $E = 210\text{GPa}$, $\nu = 0.3$, $\sigma_0 = 250\text{MPa}$ and the hardening function $\sigma_y = \sigma_0 + 2000\bar{\varepsilon}^p$ were assumed. The exact values of the parameters were not relevant from the point of view of the validation procedure. Finally, the obtained stress distributions were compared (see Fig. 2b and c). In the validation procedure no real test was considered. The distributions of σ_{yy} obtained using the procedure presented above and corresponding result of FEA are presented in Fig. 2b and c, respectively.

The time dependencies of the σ_{yy} component obtained using both methods were drawn to check the correctness of the algorithm implementation (Fig. 3). The dependencies were obtained from the stress distributions for two pairs of points with the same coordinates. The results obtained show that the DIC-based stress calculation algorithm was implemented correctly.

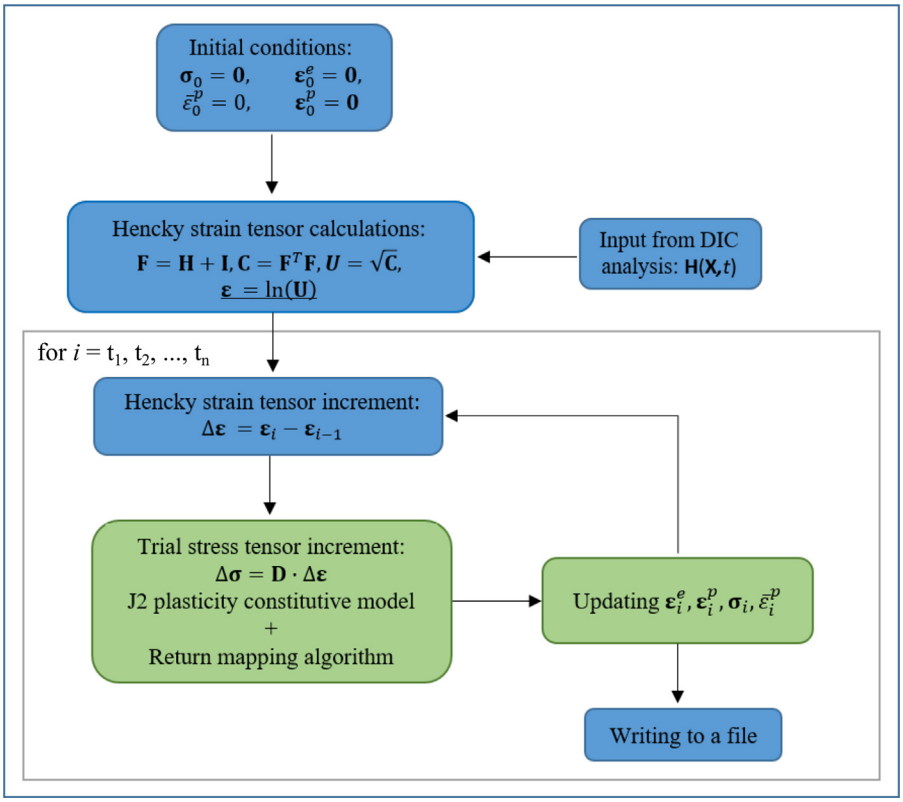

Fig. 1 – The flowchart of the DIC-based stress calculation algorithm.

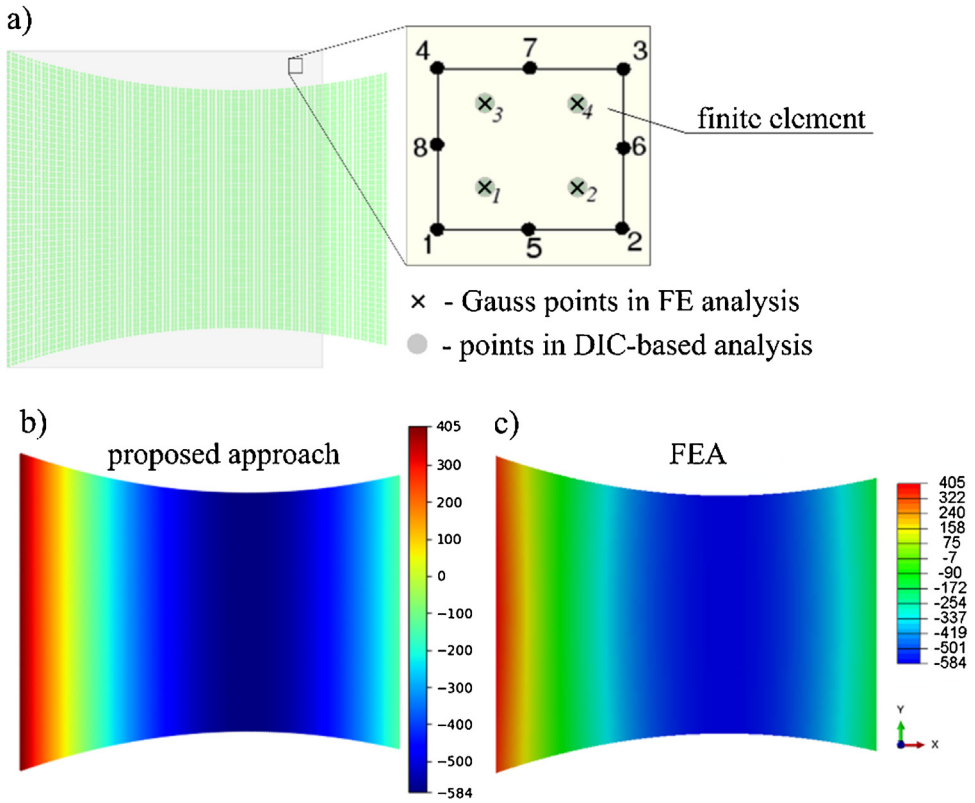

Fig. 2 – (a) The reference configuration of the 2D region used for computations (grey) and deformed configuration (green). Distributions of σ_{yy} obtained using (b) procedure presented above and (c) FEA.

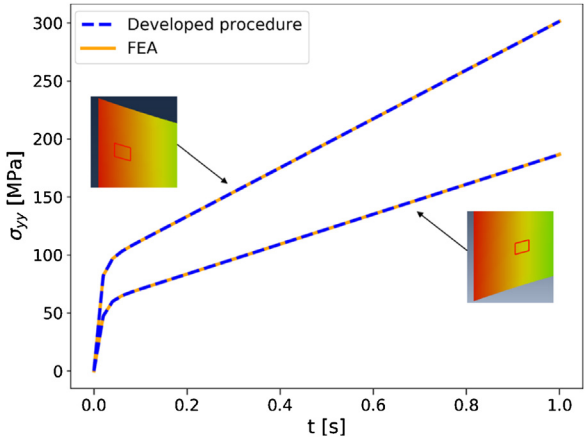

Fig. 3 – History plots of σ_{yy} obtained for the developed procedure and FEA for the points marked in the internal drawings.

3. Experimental and FEA details

The presented approach was used for determining stress distributions for experimentally measured displacement fields during uniaxial tension and simple shear tests. The results were compared with the results of numerical simulations.

The uniaxial tension and simple shear tests were performed on the samples made from 304L austenitic stainless steel. The samples were cut out from the 0.8 mm thick sheet using electro-erosion machining. The geometry and dimensions of the samples used in both tests are presented in Fig. 4a and b, respectively. In the same figures the regions of interest used in DIC and FEA are shown. The simple shear conditions were realized by eccentric compression of the specimen (Fig. 4b) using the device presented in Fig. 4d. A similar approach has been used in other studies [26,27]. The device allows analysis of the shear zones using optical system. The deformed specimen after the shear test is presented in Fig. 4c. Both experiments were carried out using MTS 858 testing machine under constant displacement rates equal to 0.015 mm/s. During the experiments, the surfaces of the specimens were covered with soot and small dots of white paint and observed using Manta G-125 camera and the sequences of images were recorded. The settings of the camera were the same for both the tension and simple shear tests (Table 1). The force and displacement of the grips of the testing machine were recorded. On the basis of the image sequences obtained, the evolutions of the displacement fields were determined using our own implementation of 2D DIC algorithm [25]. DIC analysis was performed for the square subset window 37 × 37 pixels. Then, the evolution of the DIC-based stresses was determined based on the procedure described in Section 2. The material parameters needed for the constitutive model were determined from a uniaxial

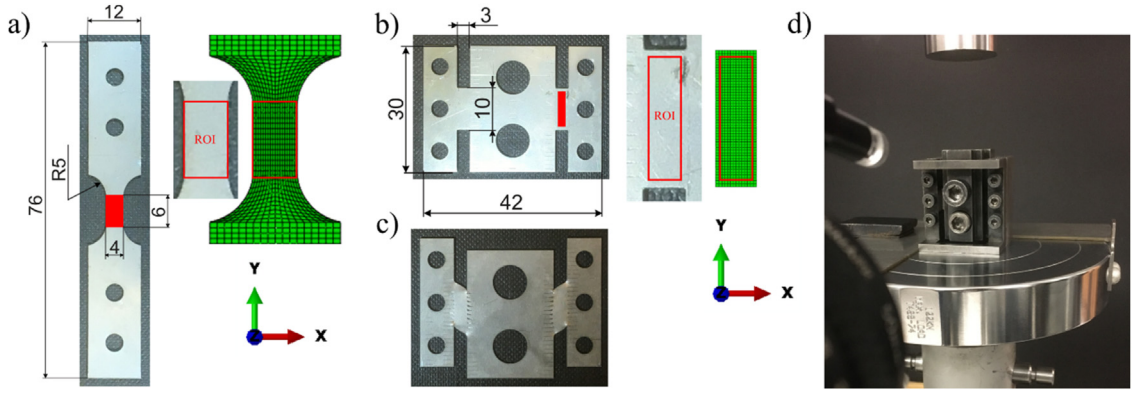

Fig. 4 – Geometry and dimensions of samples for (a) uniaxial tension and (b) simple shear. (c) The deformed specimen after shear test. (d) The device for fixing specimens for simple shear test.

Table 1 – Settings of visible range camera.

Parameter	Value
Resolution [pixel]	1292 × 964
Recording frequency [Hz]	10
Exposure time [ms]	1.5
Pixel size [μm]	9.5

tensile test: Young's modulus, $E = 190$ GPa; Poisson's ratio, 0.262; yield stress, $\sigma_0 = 240$ MPa. The hardening function in the form $\sigma_y = \sigma_0 + 640.919 \cdot (\varepsilon^p)^{0.5075} + 762.854 \cdot \varepsilon^p \cdot e^{0.4805 \cdot \varepsilon^p}$ was used.

The obtained DIC-based stress fields were compared with the FEA performed for both uniaxial tension and simple shear tests. In the first step, the geometry of the specimens was discretized (see Fig. 4a and b) and displacement boundary

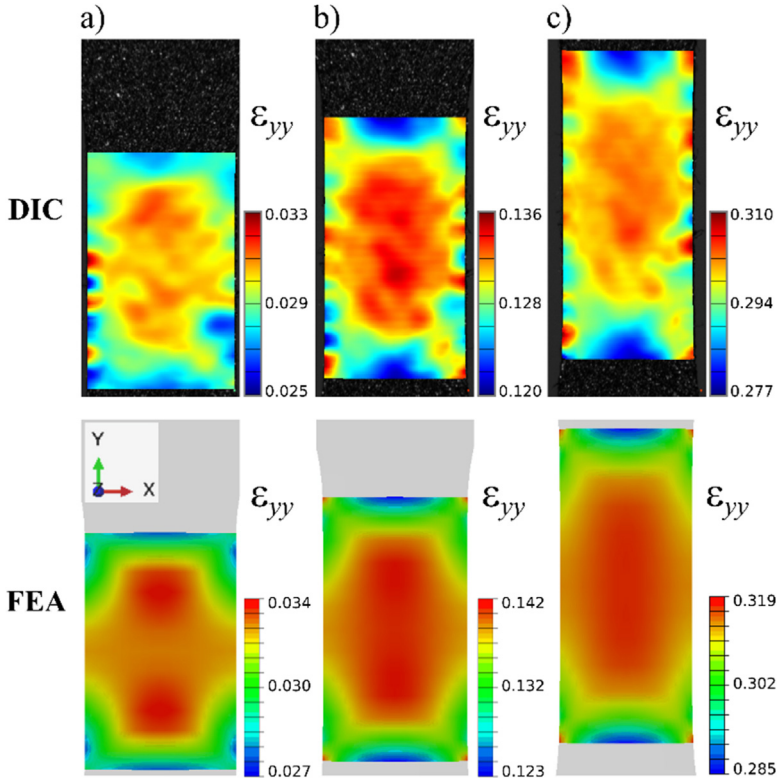

Fig. 5 – The evolution of distributions of ε_{yy} determined using a DIC-based approach and FEA for time instance (a) 20 s, (b) 100 s and (c) 250 s (end of the process).

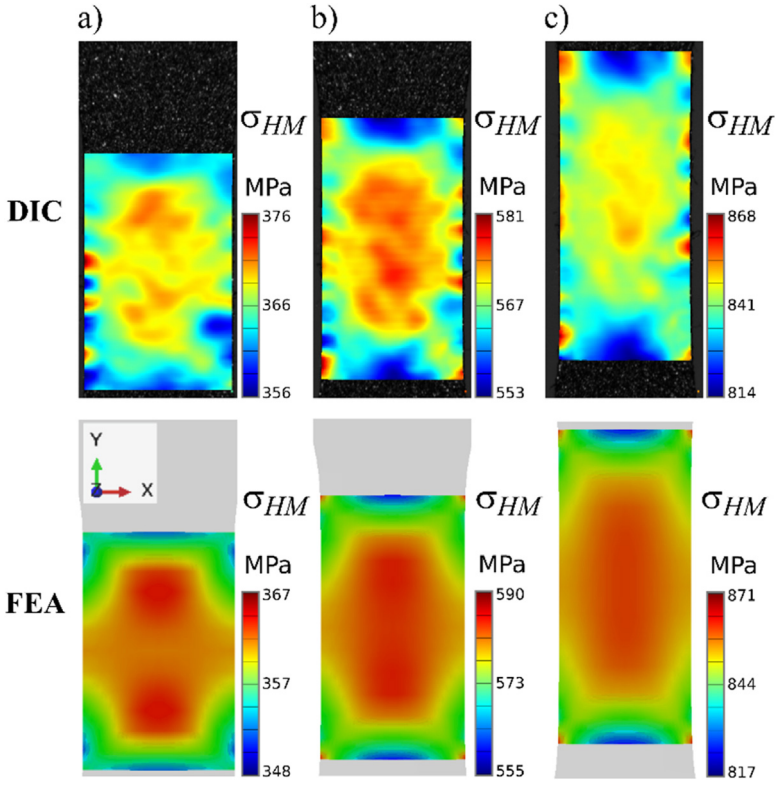

Fig. 6 – The evolution of distributions of σ_{HM} determined using a DIC-based approach and FEA for time instance (a) 20 s, (b) 100 s and (c) 250 s (end of the process).

conditions were applied according to the experimental process. For both simulations the same constitutive model and material parameters as in the DIC-based approach were assumed.

The numerical simulations of those experiments were carried out using the ABAQUS FE program. In FEA, the quasi-static equilibrium equation and elastic-plastic material model were assumed. A 20-node quadratic brick (C3D20) element type was chosen.

4. Results and discussion

First, the results of the DIC-based approach and FEA were compared for the uniaxial tension test. The evolutions of the calculated strains and stresses are presented in Figs. 5 and 6, respectively. As expected, the distributions of strain using FEA are smoother and more continuous with respect to DIC results. However, the range of strains and stresses for the DIC-based approach and FEA are very similar. The local non-uniformities observed in experimentally obtained distributions can be an effect of either uncertainty of the DIC measurement or inhomogeneity of the tested material. The peak values located at the sample boundaries are caused by poor correlation coefficients in this region (see Fig. 7).

Figs. 8 and 9 show the shear strains ε_{xy} and Huber–von Mises stresses σ_{HM}. The zone of uniform deformation is located at the centre of the sample, whereas in its upper and lower parts the values of the shear strains and Huber–von Mises stresses are significantly lower. Similar to as in the case of uniaxial tension, the experimentally obtained distributions are less smooth but their ranges are very close to those obtained by FEA. The small discrepancies between the FEA and DIC results indicate that the deformation state realized by the device for eccentric compression shown in Fig. 4d can be roughly treated as the simple shear.

On the basis of obtained stress fields, both for the DIC-based approach and FEA, the evolution of the macroscopic force was determined and compared with the force evolution measured by the testing machine. In the DIC-based approach, the evolution of stress distributions for each instant of the

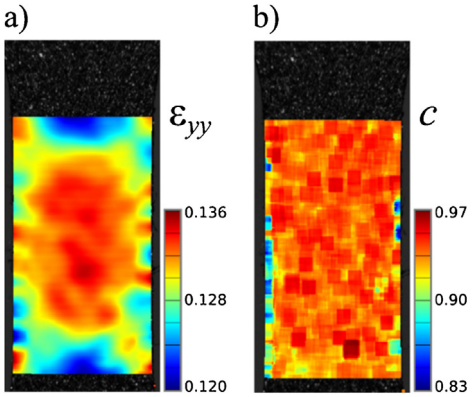

Fig. 7 – The distribution of (a) the ε_{yy} and (b) the corresponding distribution of the correlation coefficient.

deformation process were averaged over several cross-sections of the sample in the reference configuration. Due to the fact that the calculations were carried out on the reference configuration, the Cauchy stress was converted into the nominal stress, according to the following relationship:

$$\boldsymbol{\Sigma} = J\mathbf{F}^{-1}\boldsymbol{\sigma}, \tag{5}$$

where $J = \det\mathbf{F}$.

The macroscopic force was calculated as $F = \langle\Sigma\rangle A_0$ where $\langle\cdot\rangle$ denotes averaged nominal stress Σ_{yy} for uniaxial tension and Σ_{xy} for simple shear. A_0 denotes the specimen's initial cross section area. Checks were done to ensure that there were no significant discrepancies between force evolutions obtained for different cross-sections. Therefore, one lying at the sample centre was chosen as the representative for the DIC-based method and compared with the cross-sectional force evolution computed using the FE program and the one measured in the experiment. The comparisons for both uniaxial tension and simple shear are shown in Fig. 10.

For uniaxial tension (Fig. 10a) all obtained evolutions of macroscopic forces were in good agreement in both linear and non-linear domains. However, in the case of simple shear a distinct difference was observed between the FEA and experiment in the non-linear range (see Fig. 10b). The FEA significantly overestimated the value of macroscopic force, whereas the force values predicted using the proposed DIC-based approach were close to the experiment. This result can

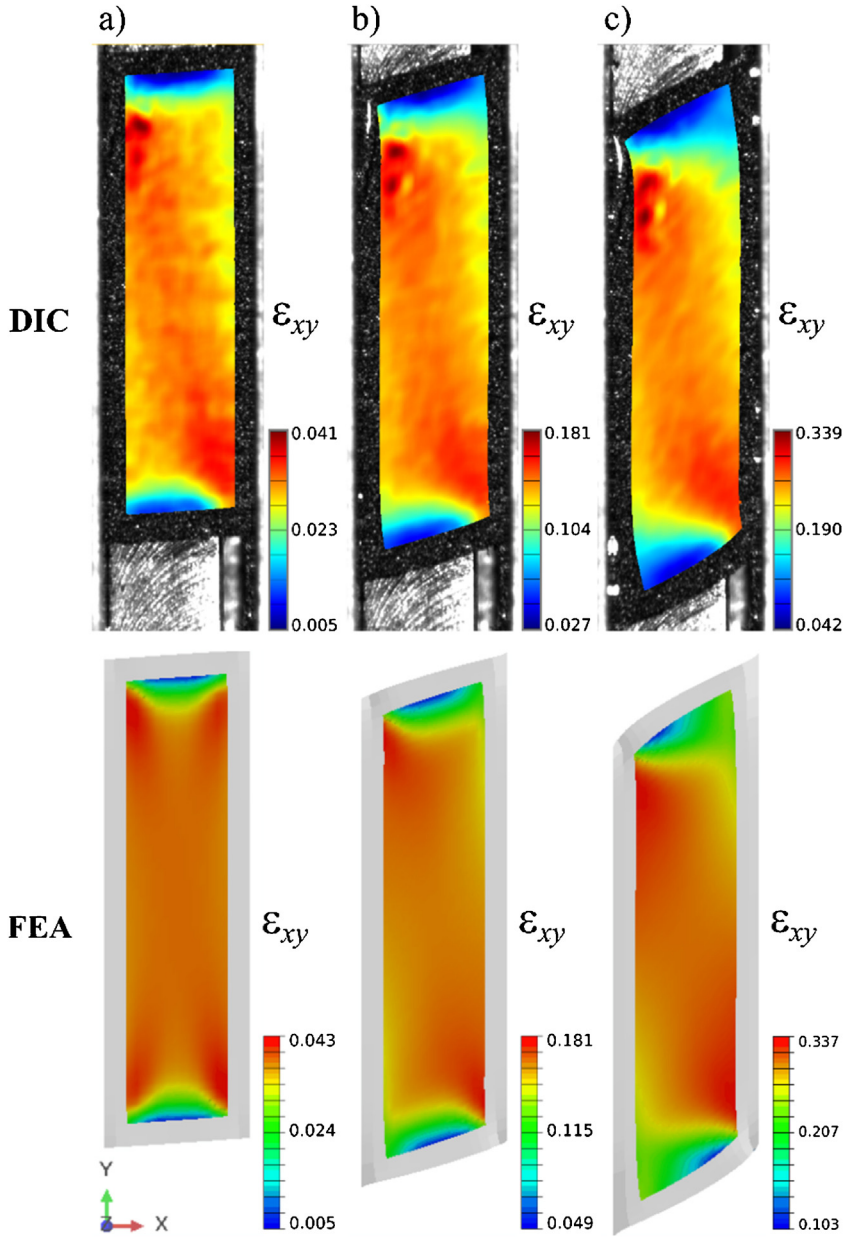

Fig. 8 – The evolution of distributions of ε_{xy} determined using a DIC-based approach and FEA for time instance (a) 25 s, (b) 85 s and (c) 160 s (end of the process).

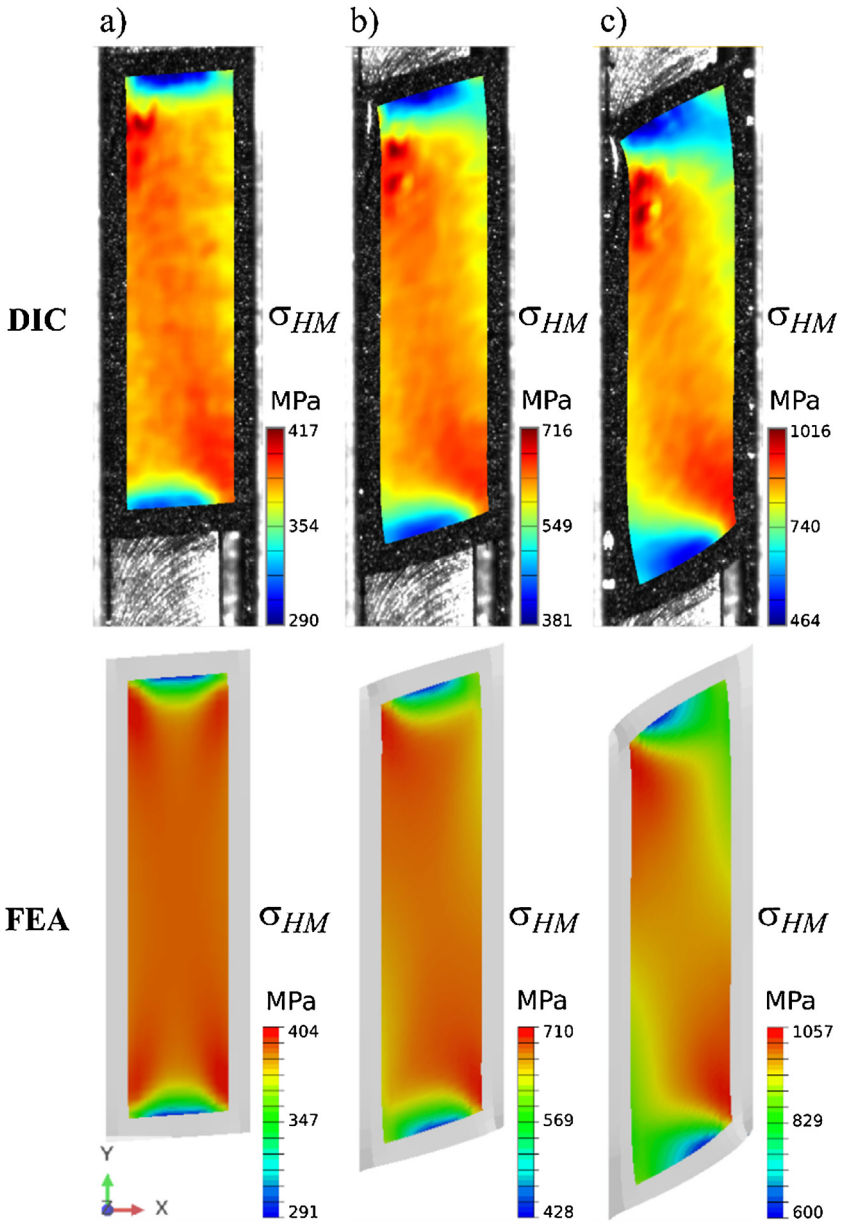

Fig. 9 – The evolution of distributions of σ_{HM} determined using a DIC-based approach and FEA for time instance (a) 25 s, (b) 85 s and (c) 160 s (end of the process).

be explained by the fact that in the DIC-based approach the strain field used for the stress calculations is measured in the experiment, which takes into account all inaccuracies that influence the deformation process (i.e. inaccuracies in sample preparation, material non-homogeneities, misalignment of the loading system, testing machine compliance, etc.). As is seen in Fig. 11, the u_x distribution measured in the experiment using DIC is not uniform, what generates strains in this direction. The prescribed displacements' boundary conditions in FEA, corresponding to the simple shear deformation, do not allow the strain components in the x direction, which seems to cause the macroscopic force overestimation in FEA. The proper formulation of boundary conditions is crucial in FEA, but difficult to define in more complex deformation states realized in the experiment. Therefore, the presented DIC-based approach, where the experimentally measured displacement field is already influenced by the experimental conditions, seems to be an adequate method for the stress field determination, especially in complex deformation processes.

The distributions of elastic ε^e_{yy}, plastic ε^p_{yy} and equivalent plastic ε^p strains obtained for the final stage of the process of uniaxial tension are presented in Fig. 12a–c. With the strain decomposition on the elastic and plastic parts and using the work conjugated measure of stress, the elastic w^e and plastic w^p works can be obtained as $w^e = 1/\rho \int \boldsymbol{\sigma} : d\boldsymbol{\varepsilon}^e$ and $w^p = 1/\rho \int \boldsymbol{\sigma} : d\boldsymbol{\varepsilon}^p$, respectively (Fig. 12d and e). From the total elastic and plastic works for a given instant of the deformation process equal to $w^e = \int_V w^e \, dV$ and $w^p = \int_V w^p \, dV$, respectively,

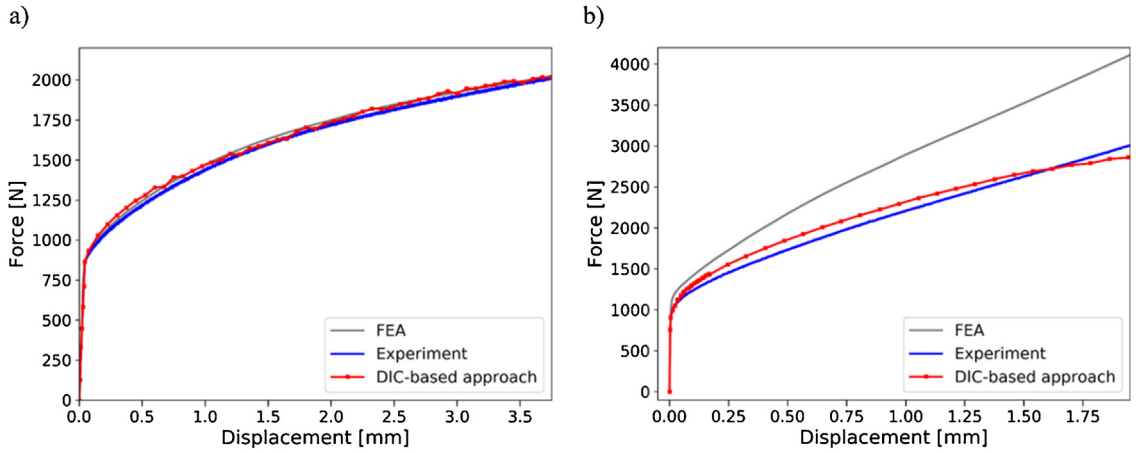

Fig. 10 – Comparison of the macroscopic force evolution obtained for FEA, a DIC-based approach and the testing machine during (a) uniaxial tension and (b) a simple shear process.

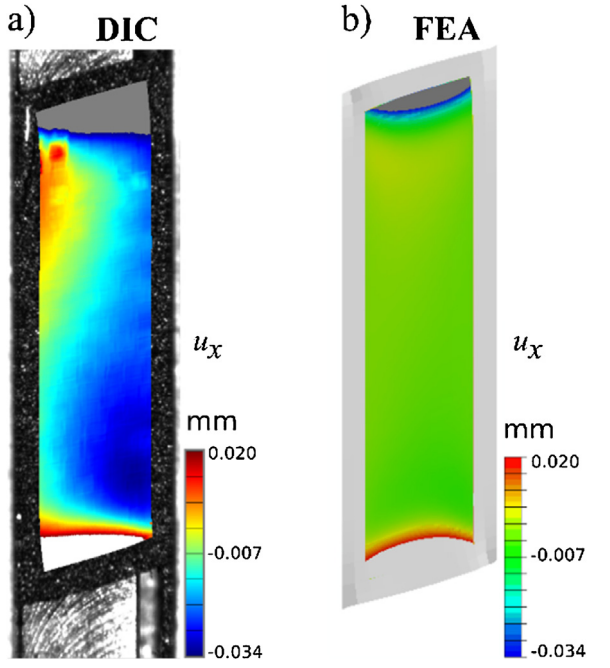

Fig. 11 – The distributions of u_x obtained for (a) a DIC-based approach and (b) FEA.

the contribution of the w^p in the total energy was calculated as $(w^p/(w^e + w^p)) \times 100\%$. In the case of uniaxial tension the contribution was equal to 98.7%.

The distributions of ε^e_{xy}, ε^p_{xy}, ε^p, w^e and w^p for the simple shear test are presented in Fig. 13. Comparison of the ε^p_{xy} and ε^p indicates that in this case the other components of the plastic strain tensor cannot be neglected (contrary to uniaxial tension). As with the uniaxial tension, the contribution of W^p in total work is approximately 99%.

5. Summary and conclusions

In the present paper, the original DIC-based stress determination method has been proposed. The developed algorithm was numerically verified with the FEA results and then implemented in the ThermoCorr DIC software. The presented approach was used for determining stress distributions for experimentally obtained displacement fields during uniaxial tension and simple shear tests and the results were compared with FEA solutions. The distributions of the DIC-based stresses were used for determining macroscopic force then the force and its FEA equivalent were compared with the force measured by the testing machine during the experiment. It

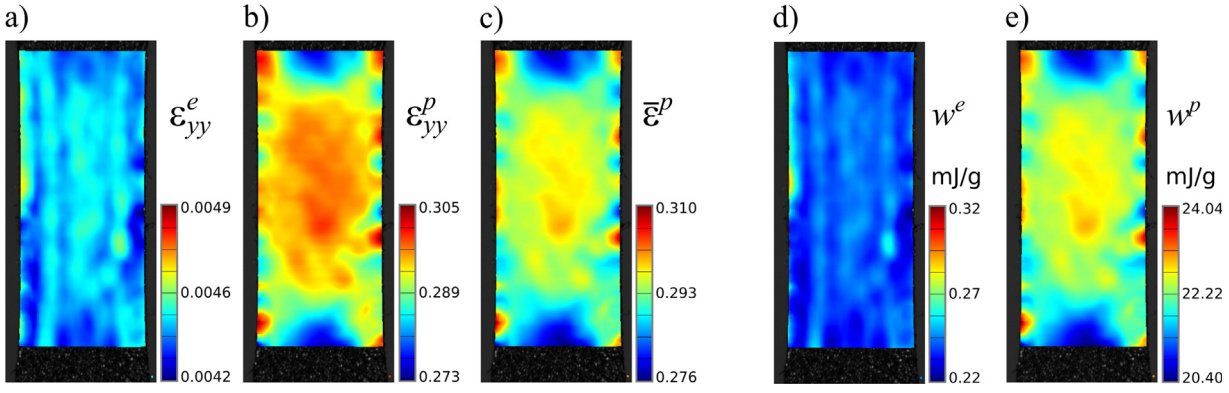

Fig. 12 – The distributions of (a) ε^e_{yy}, (b) ε^p_{yy}, (c) ε^p, (d) w^e and (e) w^p obtained for the DIC-based approach in the last moment of the uniaxial tension process.

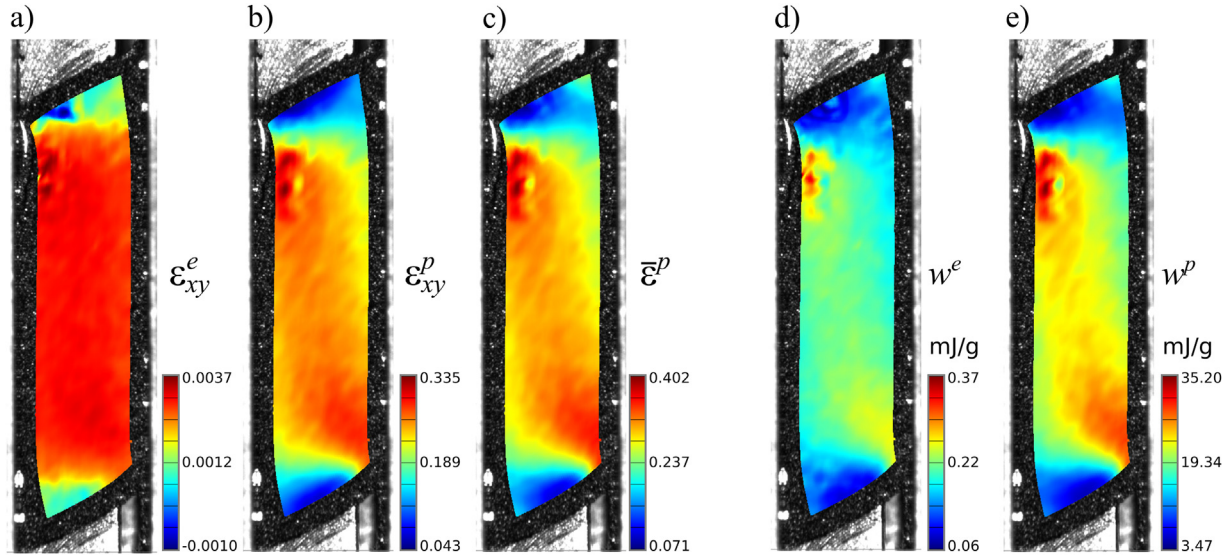

Fig. 13 – The distributions of (a) ε^e_{xy}, (b) ε^p_{xy}, (c) $\bar{\varepsilon}^p$, (d) w^e and (e) w^p obtained for the DIC-based approach in the last moment of the simple shear process.

was shown that the DIC-based approach gives significantly more accurate results with respect to FEA, especially for simple shear test, where FEA overestimates the experimentally obtained values. This result can be explained by the fact that in the DIC-based approach the strain field used for the stress calculations is measured in the experiment and takes into account all inaccuracies that influence the deformation process (i.e. inaccuracies in sample preparation, material non-homogeneities, misalignment of the loading system, testing machine compliance, etc.). None of these inaccuracies are taken into account in FE simulations. In the proposed DIC-based approach it is not necessary to define the boundary conditions, which is an advantage in relation to FEA. The distributions of elastic and plastic work were obtained on the basis of determined strain and stress fields. In further research the results will be used in the field analysis of the energy conversion during the deformation process. This will be a continuation of studies on stored energy during deformation of polycrystalline materials [18,28].

Acknowledgement

The project was funded by the National Science Centre based on the Grant Number 2012/07/D/ST8/02665.

REFERENCES

[1] T.C. Chu, W.F. Ranson, M.A. Sutton, W.H. Peters, Applications of digital-image-correlation techniques to experimental mechanics, Exp. Mech. 25 (3) (1985) 232–244.
[2] M.A. Sutton, W.J. Wolters, W.H. Peters, W.F. Ranson, S.R. McNeill, Determination of displacements using an improved digital correlation method, Image Vis. Comput. 1 (3) (1983) 133–139.
[3] H.A. Bruck, S.R. McNeill, M.A. Sutton, W.H. Peters, Digital image correlation using Newton–Raphson method of partial differential correction, Exp. Mech. 29 (3) (1989) 261–267.
[4] J. Harvent, B. Coudrin, L. Brèthes, J.J. Orteu, M. Devy, Shape measurement using a new multi-step stereo-DIC algorithm that preserves sharp edges, Exp. Mech. 55 (1) (2015) 167–176.
[5] T. Gajewski, T. Garbowski, Calibration of concrete parameters based on digital image correlation and inverse analysis, Arch. Civil Mech. Eng. 14 (2014) 170–180.
[6] B. Pan, K. Qian, H. Xie, A. Asundi, Two-dimensional digital image correlation for in-plane displacement and strain measurement: a review, Meas. Sci. Technol. (2009), http://dx.doi.org/10.1088/0957-0233/20/6/062001.
[7] C.C.B. Wang, N.O. Chahine, C.T. Hung, G.A. Ateshian, Optical determination of anisotropic material properties of bovine articular cartilage in compression, J. Biomech. 36 (3) (2003) 339–353.
[8] O. Orella, J. Vuorinena, J. Jokinena, H. Kettunenb, P. Hytönenb, J. Turunenb, M. Kanervaa, Characterization of elastic constants of anisotropic composites in compression using digital image correlation, Compos. Struct. 185 (2018) 176–185.
[9] Y. Cai, Q. Zhang, S. Yang, S. Fu, Y. Wang, Experimental study on three-dimensional deformation field of Portevin–Le Chatelier effect using digital image correlation, Exp. Mech. 56 (7) (2016) 1243–1255.
[10] N.A. Sène, P. Balland, K. Bouabdallah, Experimental study of Portevin–Le Châtelier bands on tensile and plane strain tensile tests, Arch. Civil Mech. Eng. 18 (1) (2018) 94–102.
[11] F. Hild, A. Bouterf, S. Roux, Damage measurements via DIC, Int. J. Fract. 191 (1–2) (2015) 77–105.
[12] M. Maj, W. Oliferuk, Analysis of plastic strain localization on the basis of strain and temperature fields, Arch. Metall. Mater. 57 (4) (2012) 1111–1116.
[13] J. Agirre, L. Galdos, E. Saenz de Argandoña, J. Mendiguren, Hardening prediction of diverse materials using the Digital Image Correlation technique, Mech. Mater. 124 (2018) 71–79.
[14] B.V. Farahani, J. Belinha, R. Amaral, P.J. Tavares, P. Moreira, A digital image correlation analysis on a sheet AA6061-T6 bifailure specimen to predict static failure, Eng. Fail. Anal. 90 (2018) 179–196.
[15] D. Gerbig, A. Bower, V. Savic, L.G. Hector Jr., Coupling digital image correlation and finite element analysis to determine

constitutive parameters in necking tensile specimens, Int. J. Solids Struct. 97–98 (2016) 496–509.
[16] D.V. Nelson, A. Makino, T. Schmidt, Residual stress determination using hole drilling and 3D image correlation, Exp. Mech. 46 (2006) 31–38.
[17] J.D. Lord, D. Penn, P. Whitehead, The application of digital image correlation for measuring residual stress by incremental hole drilling, Appl. Mech. Mater. 13–14 (2008) 65–73.
[18] W. Oliferuk, M. Maj, K. Zembrzycki, Determination of the energy storage rate distribution in the area of strain localization using infrared and visible imaging, Exp. Mech. 55 (2015) 753–760.
[19] F. Toussaint, L. Tabourot, P. Vacher, Experimental study with a Digital Image Correlation (DIC) method and numerical simulation of an anisotropic elastic-plastic commercially pure titanium, Arch. Civil Mech. Eng. 8 (3) (2008) 131–143.
[20] S. Marth, H.-Å. Häggblad, M. Oldenburg, R. Östlund, Post necking characterisation for sheet metal materials using full field measurement, J. Mater. Process. Technol. 238 (2016) 315–324.
[21] A. Brosius, N. Küsters, M. Lenzen, New method for stress determination based on digital image correlation data, CIRP Ann. Manuf. Technol. 67 (2018) 269–272.
[22] P.F. Luo, Y.J. Chao, M.A. Sutton, W.H. Peters, Accurate measurement of three-dimensional deformations in deformable and rigid bodies using computer vision, Exp. Mech. 33 (2) (1993) 123–132.
[23] B.K. Bay, T.S. Smith, D.P. Fyhrie, M. Saad, Digital volume correlation: three-dimensional strain mapping using X-ray tomography, Exp. Mech. 39 (3) (1999) 217–226.
[24] J.C. Simo, R.L. Taylor, A return mapping algorithm for plane stress elastoplasticity, Int. J. Numer. Methods Eng. 22 (1986) 649–670.
[25] M. Nowak, M. Maj, Determination of coupled mechanical and thermal fields using 2D digital image correlation and infrared thermography: numerical procedures and results, Arch. Civil Mech. Eng. 18 (2018) 630–644.
[26] S.P. Gadaj, W.K. Nowacki, E.A. Pieczyska, Changes of temperature during the simple shear test of stainless steel, Arch. Mech. 48 (4) (1996) 779–788.
[27] E.A. Pieczyska, S.P. Gadaj, W.K. Nowacki, J. Luckner, H. Tobushi, Martensite and reverse transformation during simple shear of NiTi shape memory alloy, Strain 45 (2009) 93–100.
[28] W. Oliferuk, M. Maj, Stress–strain curve and stored energy during uniaxial deformation of polycrystals, Eur. J. Mech. A-Solids 28 (2) (2009) 266–272.